

Spatial distribution of degradation and deforestation of palm swamp peatlands and associated carbon emissions in the Peruvian Amazon

List of Authors: Matthew Marcus^{1*}, Kristell Hergoualc'h², Euridice Honorio Coronado³, Víctor Hugo Gutiérrez-Vélez¹

¹Temple University Department of Geography and Urban Studies, Philadelphia, PA, USA

²Center for International Forestry Research (CIFOR), Lima, Peru and Agricultural Research Centre for International Development (CIRAD), Montpellier, France

³School of Geography and Sustainable Development, University of St Andrews, St Andrews, KY16 9AL, United Kingdom

*** Corresponding author:** Matthew Marcus. Temple University Department of Geography and Urban Studies. 308 Gladfelter Hall, 1115 Polett Walk, Philadelphia, PA 19122 USA

Email: matthew.marcus@temple.edu

Supplementary Methods

SI Methods 1. Climate in the study area

The climate near Iquitos in Loreto has a mean annual air temperature of 26°C and receives 3,100 mm yr⁻¹ of precipitation. The Loreto region has no dry season, i.e., no month with less than 100 mm of rain, although lower precipitation is observed from April through October than during the rest of the year (Marengo, 1998). Pucallpa in the Ucayali region has a mean annual air temperature of 25°C and has a dry season between the months of June and August. The precipitation rate varies from 1,500 to 2,500 mm yr⁻¹ (Barbaran-Garcia, 2000; Fujisaka et al., 2000).

SI Methods 2. Remote sensing image sources and pre-processing

The Landsat data was used to produce three other data sources that were included as input data for the classification: the Normalized Difference Vegetation Index (NDVI), the Normalized Difference Water Index (NDWI), and the Modified Soil-Adjusted Vegetation Index (MSAVI). This last one was found to be useful for tropical forest environments (Matricardi et al., 2010).

ALOS-PALSAR data for 2007 and 2018, of HH and HV polarization, were acquired from the Japanese space agency (JAXA). The raw data were resampled from 25 m native resolution to 30 m resolution. The 2007 and 2018 PALSAR mosaics were subjected to a Lee de-

46 speckle filter using the Sentinel Application Platform (SNAP) software. A Digital Elevation
47 Model (DEM) was included as a data source for the classification, acquired from the Shuttle
48 Radar Topography Mission (SRTM) of 1-arc second (NASA JPL, 2013). We also used canopy
49 height data for 2018, derived from the GEDI LiDAR instrument, (Potapov et al., 2020). This
50 source was used to help distinguish between different forest types known to have different
51 vegetation physiognomy, such as pole forests that are dominated by thin trees with lower heights
52 compared to surrounding tree-dominated ecosystems (Draper et al., 2018; Honorio Coronado et
53 al., 2021).

54
55 Forty-two high resolution images of 0.5 m resolution were used for the collection of
56 calibration and validation data for image classification (see Table SI 4). Twenty-three images
57 were acquired from Planet Labs, two from the Pleiades sensor, three from the Quickbird sensor,
58 six from the WorldView1 sensor, six from the WorldView2 sensor, and two from the
59 WorldView4 sensor. They were acquired during the years 2018, 2019 and 2020 to produce
60 reference data for the 2018 classification, and during the years 2005, 2008 and 2009 for
61 validating the 2007 map. The images were selected based on their quality (low cloud cover) and
62 their representativeness of heterogenous portions of the landscape to best discern different land
63 covers. Planet Labs images were deliberately selected to capture areas where more training data
64 was needed to better distinguish palm swamps from other land cover classes in complex
65 landscapes. For example, several high-resolution images were acquired for the lower Tigre
66 region where land cover is heterogenous, with a mix of pole forest, palm swamp and seasonally
67 flooded forest. Finally, high-resolution imagery from Google Earth (Google, 2021) was used
68 wherever available.

69
70 In order to produce a classification for the year 1990, manually produced mosaics for
71 1990 and 2018 were created. The 2018 training data used to classify the 2018 ARD mosaics
72 were applied to the 2018 manually produced mosaic to produce a random forest classifier that was
73 then applied to the 1990 mosaic. Images for the manually-produced mosaics were selected from
74 the driest months (May-November) for the years 1990 and 2018, plus or minus one year when
75 data filling was necessary (Table SI 2). Pre-processing of the 1990 imagery, and the 2018
76 manually-produced mosaic, consisted of cloud removal, image normalization, and image
77 reprojection and alignment. Radiometric normalization was applied using a probabilistic
78 approach to identify pseudo-invariant targets (Gutierrez-Velez et al., 2021). Clouds were masked
79 out of the Landsat images using the data contained in the quality assurance layer included in the
80 Landsat dataset and then filled out with data from the dry season in the reference year plus or
81 minus one year.

82
83
84
85

84 **SI Methods 3. Zone Stratification**

86 The study area was stratified into six zones for classification based on river basins (Figure SI 1).
87 From northeast to southwest, (1) the Putumayo-Amazonas zone includes the Putumayo River
88 and surroundings, (2) the Amazonas zone encompasses the Amazon river and its flood plain, (3)
89 the Napo-Tigre zone is the northern section encompassing the Napo river, (4) the Pastaza-
90 Marañón zone contains the area of the basin north of the Marañón river, (5) the Marañón-Ucayali

91 zone contains the area of the basin south of the Marañón river and includes the Pacaya-Samiria
92 National Reserve, and (6) the zone in the south covers the area along the Ucayali river.

93
94 The stratification was done for three reasons. First, the large size of the study area
95 requires significant computational power, which was best allocated by breaking up the image
96 into smaller areas. Second, the southern region is a landscape with heterogenous landcover types
97 and therefore classification required the discrimination between land covers nearby the wetland
98 areas that only exist in specific sectors within the study area, such as secondary forest and oil
99 palm plantation. Finally, the elevation of the landscape is a key data source in producing an
100 accurate classification, however, applying the elevation model to the entire study area introduces
101 noise in the downgradient portion of the study area (in the northeastern section, including the
102 Napo-Tigre and Amazonas zones). This is because a relatively high elevation land down the
103 gradient may be equivalent in altitude to a relatively low elevation land up gradient. For
104 example, the Pastaza-Marañón and Marañón-Ucayali are considered two different zones based
105 on an early classification which showed that the terra firme and seasonally flooded dominated
106 areas within these basins are unique spectrally and differ in their topography. Separating these
107 two zones resulted in a higher classification accuracy compared to considering the entire area as
108 one zone.

109
110 The six zones overlap in certain places (e.g. in the lower Tigre River area) to include in
111 each zone a sufficient number of training polygons per class for land cover classification. The
112 final classification map resulted from the merging of the six zones in the following order:
113 Marañón-Ucayali, Pastaza-Marañón, Amazonas, Napo-Tigre, Putumayo-Amazonas, and
114 Ucayali. The order was chosen based on the accuracy of the peat-forming classes. Zones with a
115 higher accuracy were ranked higher for merging and determined the class assigned to
116 overlapping areas.

117 **SI Methods 4.** Training Data Collection

118
119 Training data consisted of 1,444 polygons drawn across the zones (Table SI 4) through visual
120 interpretation of high-resolution images and Google Earth imagery (Google, 2021) (Figure SI 2),
121 and of false color composites using the Landsat and PALSAR data. Polygons were drawn for the
122 following peat-forming classes: palm swamp of high, medium and low density, herbaceous
123 swamp, and pole forest; and for the following non-peat-forming classes: seasonally flooded
124 forest, *terra firme* forest, pasture, lake, river, sand bank, secondary forest, and urban areas. The
125 discrimination was largely based on the unique spectral response of some classes in different
126 Red-Green-Blue (RGB) band combinations. Seasonally flooded forest was not considered a peat-
127 forming class given the limited occurrence of peat in this type of forest (Honorio Coronado et al.,
128 2021). Indeed, Hastie et al. (2022) estimated that only 2% of seasonally flooded forests overlie
129 peat.

130
131
132 The palm swamp class was disaggregated by density of *M. flexuosa* palms. Low density
133 was defined as a swamp with a canopy consisting of less than one-third of *M. flexuosa* where
134 crowns never overlapped (Figure SI 2A). Medium density was defined as a canopy consisting of
135 approximately one to two-third of *M. flexuosa* with canopy breaks including other vegetation,
136 both herbaceous vegetation and trees (Figure SI 2B). High density was defined as a swamp with

137 an unbroken canopy dominated almost entirely by *M. flexuosa* individuals (Figure SI 2C). Palm
138 swamp classes were distinguished from other forest types by the brightness of the pixels when
139 observed with the false color composite of the near infra-red (NIR), RGB bands corresponding to
140 bands 5, 4, 3 in Landsat 8 (Figure SI 3A). Different densities of *M. flexuosa* were distinguished
141 by using high-resolution imagery.

142
143 Herbaceous swamps were typically found in open areas with scattered *M. flexuosa* in the
144 high-resolution images (Figure SI 2D). They presented as bright pink in the Landsat NIR, red,
145 green false color composite. Pole forests which are dominated by thin trees with the occasional
146 presence of *M. flexuosa* at low densities (Figure SI 2E) appeared similar to palm swamps, but
147 slightly browner in the 5, 4, 3 false color composite (Figure SI 3A). Training data for pole forest
148 was collected using eight high-resolution images acquired from the region surrounding the Tigre,
149 Tapiche, Napo, Nanay, and Amazon rivers where homogenous stands of pole forest and white
150 sand forests (with similar physiognomy to pole forests) have been reported (Garcia-Villacorta et
151 al., 2003; Draper et al., 2014; Palacios et al., 2016; Honorio Coronado et al., 2021).

152
153 Differences between seasonally flooded forest and *terra firme* forest were relatively clear
154 in the Landsat NIR, Red and Green band combination (Figure SI 3B). Seasonally flooded forests
155 appeared as a bright greenish-yellow and were located close to rivers and throughout the
156 Marañón-Ucayali zone, while terra firme forest appeared as a dark green. Pasture is a trivial class
157 that mostly exists around small villages outside of wetlands. It appeared as a light pink in the 5,
158 4, 3 composite. Secondary forest, also a trivial class, only occurred in the Ucayali region and
159 resulted mostly of terra firme forest regrowth after deforestation (Figure SI 3C).

160
161 An independent validation dataset of 204 polygons were also drawn from high-resolution
162 images acquired in or around 2007 but this was impossible for 1990 when high-resolution
163 validation data were inexistant.

164
165 **SI Methods 5.** Image classification, classification post-processing and classification accuracy
166 assessment

167
168 Land cover classification was performed using the packages raster (Hijmans, 2020) and
169 RSToolbox (Leutner, 2019) available under the R programming environment (R Core Team,
170 2022). Input raster data and ground-truthing data were used to train a random forest classification
171 algorithm. The parameters of the algorithm were set to 1000 samples with a “tuneLength” setting
172 of 3, meaning that 3 bands were evaluated at each node per decision tree. The 2018 map was
173 classified using 70% of the training polygons randomly selected from the database and the
174 Landsat, PALSAR, DEM, and spectral index data (Table SI 3). The classification algorithm was
175 calibrated both with and without PALSAR and canopy height data using the 2018 mosaic and
176 training polygons. The model with all bands was used to produce the map for 2018. The model
177 with all data except for canopy height was applied to 2007. The model without PALSAR data
178 was applied to the 1990 images for when PALSAR data did not exist.

179
180 Each classification was subjected to a 3x3 majority filter to correct the “salt-and-pepper
181 effect” in randomly dispersed errant pixels. We also implemented a temporal filter to correct for
182 unlikely pixel transitions (Roberts et al., 2002; Gutierrez-Velez and DeFries 2013). Because the

183 training data was collected over the 2018 image, we assumed the 2018 classification to be the
 184 most accurate and used it as a benchmark map to apply the temporal filter. For instance, we
 185 assumed that over the observation periods (1990-2007 and 2007-2018), the density of *M.*
 186 *flexuosa* in palm swamps would not increase as recovery from degradation takes longer than 17
 187 years (1990-2007) or 11 years (2007-2018) (Holm et al., 2008). This assumption is supported by
 188 the observation that degraded stands of *M. flexuosa* with skewed male to female ratios from
 189 selective felling of females produce fewer seedlings, hampering recruitment (Horn et al., 2012;
 190 Endress et al., 2013). Table SI 5 presents corrected transitions.

191
 192 **SI Methods 6.** Calculation of emissions uncertainty using the Gaussian error propagation
 193 method

194
 195 Below are two examples of how the Gaussian error propagation method was applied for
 196 computing uncertainty of emissions.

197
 198 Example of propagation by quadrature of absolute errors for addition

199
 200 C emissions from degradation over 1990-2018 was computed as:

201
 202 $C \text{ emissions}_{\text{degradation 1990-2018}} = C \text{ emissions}_{\text{degradation 1990-2007}} + C \text{ emissions}_{\text{degradation 2007-2018}}$
 203 Where $C \text{ emissions}_{\text{degradation 1990-2007}}$ are 14.1, and $C \text{ emissions}_{\text{degradation 2007-2018}}$ are 12.3,
 204 $C \text{ emissions}_{\text{degradation 1990-2018}} = 26.3$ (with rounding) Tg

205
 206 The standard error of these emissions was computed as:

207 $SE_{C \text{ emissions}_{\text{degradation 1990-2018}}} = \text{SQRT} (SE_{C \text{ emissions}_{\text{degradation 1990-2007}}}^2 + SE_{C \text{ emissions}_{\text{degradation 2007-2018}}}^2)$

208
 209 Where $SE_{C \text{ emissions}_{\text{degradation 1990-2007}}} = 2.6$, and $SE_{C \text{ emissions}_{\text{degradation 2007-2018}}} = 2.4$
 210 $SE_{C \text{ emissions}_{\text{degradation 1990-2018}}} = \text{SQRT}(2.6^2 + 2.4^2) = 3.5$

211
 212 Example of propagation by quadrature of relative error for multiplication

213
 214 C emissions of AGB loss resulting from degradation for the transition palm swamp high density
 215 to palm swamp medium density over the period 1990-2007 was computed as:

216
 217 $C \text{ emission}_{\text{AGB high density to medium density 1990-2007}} = \text{Area}_{\text{high density to medium density 1990-2007}} \times (\text{AGB}_{\text{high density}} - \text{AGB}_{\text{medium density}})$

218
 219 Where $\text{Area}_{\text{high density to medium density 1990-2007}}$ is 56251.29 ha, $\text{AGB}_{\text{high density}}$ is 75.6 and $\text{AGB}_{\text{medium density}}$ is 67.3 Mg C ha⁻¹,

220
 221 $C \text{ emission}_{\text{AGB high density to medium density 1990-2007}} = 56251.29 \text{ ha} \times (75.6 \text{ Mg C ha}^{-1} - 67.3 \text{ Mg C ha}^{-1}) = 0.47 \text{ TgC}$

222
 223
 224 The standard error of these emissions was computed as:

225
 226 $SE_{C \text{ emission}_{\text{AGB high density to medium density 1990-2007}}} = C \text{ emission}_{\text{AGB high density to medium density 1990-2007}} \times \text{SQRT} [(SE_{\text{Area}_{\text{high density to medium density 1990-2007}}} / \text{Area}_{\text{high density to medium density 1990-2007}})^2 + (SE_{(\text{AGB}_{\text{high density}} - \text{AGB}_{\text{medium density}})})^2]$

229 Where $SE_{\text{Area high density to medium density 1990-2007}}$ is 3902, and $SE_{\text{(AGB high density - AGB medium density)}}$ is the
 230 standard error of the difference in AGB C stocks between palm swamp high density and palm
 231 swamp medium density. The latest was computed as:

232
 233 $SE_{\text{(AGB high density - AGB medium density)}} = \text{SQRT}(SE_{\text{AGB high density}}^2 + SE_{\text{AGB medium density}}^2)$
 234 Where $SE_{\text{AGB high density}}$ is $\text{SQRT}(4.3^2 + 3.8^2) = 5.8$

235
 236

237 **Supplementary Tables**

238

239 **Table SI 1.** ARD tiles used for 2018 and 2007 mosaics

240

69W	70W	71W	72W	73W	74W	75W	76W	77W
069W_0	070W_0	071W_0	072W_0	073W_0	074W_0	075W_0	076W_0	077W_0
4S	2S	2S	2S	0S	0S	0S	1S	2S
	070W_0	071W_0	072W_0	073W_0	074W_0	075W_0	076W_0	077W_0
	3S	3S	3S	1S	1S	1S	2S	3S
	070W_0	071W_0	072W_0	073W_0	074W_0	075W_0	076W_0	077W_0
	4S	4S	4S	2S	2S	2S	3S	4S
			072W_0	073W_0	074W_0	075W_0	076W_0	077W_0
			5S	3S	3S	3S	4S	5S
				073W_0	074W_0	075W_0	076W_0	
				4S	4S	4S	5S	
				073W_0	074W_0	075W_0	076W_0	
				5S	5S	5S	6S	
				073W_0	074W_0	075W_0		
				6S	6S	6S		
				073W_0	074W_0	075W_0		
				9S	7S	7S		
				073W_1	074W_0			
				0S	8S			
					074W_0			
					9S			
					074W_1			
					0S			

241

242 **Table SI 2.** Landsat scenes used to produce the 1990 classification

243

244 In the absence of ARD imagery for the year 1990, the 2018 images were used to produce a
 245 random forest classification that was applied to the 1990 mosaic. The Table presents Path/Row,
 246 and dates of images acquired for each Landsat scene.

247

Mosaic Year	Path/Row	Ref Date	Date 2	Date 3	Date 4	Date 5	Date 6
2018	7.61	7/13/2017	8/30/2017	9/18/2018			
2018	7.62	7/13/2017	8/14/2017	8/30/2017	9/7/2020		
2018	7.63	7/13/2017	8/30/2017	10/1/2017	7/16/2018	9/7/2020	8/6/2020
2018	7.64	7/13/2017					

2018	7.65	7/13/2017	7/29/2017	
2018	7.66	7/16/2018	6/30/2018	10/1/2017
2018	6.62	10/29/2018	9/11/2018	
2018	6.63	10/29/2018		
2018	6.64	10/29/2018	9/11/2018	
2018	6.65	6/23/2018	9/14/2019	
2018	6.66	6/23/2018	9/11/2018	
2018	6.67	6/23/2018		
2018	8.61	7/20/2017	6/21/2018	8/24/2018
2018	8.62	7/20/2017	9/25/2018	8/24/2018
2018	8.63	7/20/2017	9/25/2018	7/10/2019
2018	8.64	7/20/2017	9/25/2018	7/10/2019
2018	5.62	7/20/2017	9/25/2018	7/10/2019
2018	5.63	7/2/2018	8/6/2019	
1990	4.63	9/13/1989	8/28/1989	
1990	4.62	9/13/1989		
1990	5.62	7/26/1990	9/28/1990	
1990	5.63	9/7/1990	9/4/1989	
1990	6.62	8/26/1989	9/11/1989	6/7/1989
1990	6.63	8/26/1989	9/11/1989	
1990	6.64	8/26/1989	9/11/1989	
1990	6.65	8/26/1989	7/9/1989	
1990	6.66	8/26/1989		
1990	6.67	8/26/1989		
1990	7.61	7/19/1990	6/20/1991	8/20/1990
1990	7.62	7/24/1989	8/25/1989	9/2/1989
1990	7.63	7/24/1989	6/14/1989	6/6/1992
1990	7.64	7/24/1989	8/25/1989	6/14/1989
1990	7.65	8/25/1989	7/16/1989	
1990	7.66	8/25/1989	7/24/1989	7/16/1989
1990	8.6	10/1/1991		
1990	8.61	7/26/1990		
1990	8.62	7/26/1990		
1990	8.63	7/26/1990	9/28/1990	
1990	8.64	7/26/1990	9/28/1990	
1990	9.62	11/11/1989		
1990	9.63	11/11/1989		

249
250

Table SI 3. Remote sensing images and ancillary products used in producing classifications

Data	Source	Bands	Native Resolution (m)	Purpose
Landsat 7 & 8/ARD	NASA, UMD	3-7 (Landsat 8)	30	Classification 2018
Landsat 5 & 7/ARD	NASA, UMD	2-5,7	30	Classification 2007
Landsat 5	NASA	2-5,7	30	Classification 1990
NDVI, NDWI, MSAVI	Landsat 5, 7 & 8/ARD		30	Classification all years
ALOS-PALSAR	JAXA	HH, HV	25	Classification 2007, 2018
DEM	NASA – SRTM		~30 (1-arc second)	Classification all years
Canopy height	NASA – GEDI		30	Classification 2018
High Resolution	Pleiades, WorldView1, WorldView2,		0.5	Calibration, validation
	WorldView4, Planet Labs, Quickbird		0.5	
Google Earth	Google, 2021		NA	Calibration, validation
Peat map	Hastie et al. (2022)		100	Peat area delineation

251
252
253
254
255
256

Table SI 4. Number of polygons drawn in the six classification zones per land cover class for the year 2018. * indicates peat forming classes. PS: Palm swamp, HS: Herbaceous swamp, PF: Pole forest, SFF: Seasonally Flooded Forest

Class	Putumayo Amazonas	Amazonas	Napo Tigre	Pastaza Marañón	Marañón Ucayali	Ucayali	Total per class
*PS high density	5	13	19	69	28	12	146
*PS medium density	9	17	43	98	32	3	202
*PS low density	24	25	53	78	20	5	205
*HS	7	6	10	23	16	30	92
*PF	6	42	75	36	10	0	169
SFF	17	34	35	9	35	43	173
Terra Firme Forest	30	7	29	109	26	5	206
Pasture	12	6	0	2	12	7	39
Water	20	20	16	20	20	14	110

Sand Bank	7	7	6	10	9	5	44
Urban	6	7	7	5	3	17	45
Secondary Forest	0	0	0	0	0	13	13
Total per zone	143	184	293	459	211	154	1,444

257
258
259
260
261
262
263
264
265
266

Table SI 5. Class correction for unlikely transitions. PS: Palm swamp, PF: Pole forest

Some transitions were assessed as unlikely to occur, such as an increase in palm density. For these transitions, we assigned to the year previous to the observation year the same class identified in the observation year. For example, a pixel of PS high density in 2018 and PS medium density in 2007 had its 2007 pixel reassigned to PS high density.

Class in observation year	Class in year previous to observation year	Corrected class in year previous to observation year
PS high density	PS medium density	PS high density
PS high density	PS low density	PS high density
PS medium density	PS low density	PS medium density
PS of any density	No palm	PS density of observation year
Terra firme	PS or PF	Terra firme

267

268 **Table SI 6.** C stocks \pm SE (Mg C ha⁻¹) in the above-ground biomass (AGB), below-ground
 269 biomass (BGB) and the soil of ecosystems on peat. PS: Palm swamp, HS: Herbaceous swamp,
 270 PF: Pole forest
 271

Peat ecosystem	AGB	BGB	Soil	Assumption and references
PS high density	75.6 \pm 4.3	22.5 \pm 2.4	647.8 \pm 41.0	Undegraded PS. Values from Honorio Coronado et al. (2021)
PS medium density	67.3 \pm 3.8	20.0 \pm 2.1	647.8 \pm 41.0	Biomass stock assumed to be similar to that of a PS of medium degradation or 89% the stock in PS high density according to Hergoualc'h et al. (2017). Peat C stocks conservatively assumed to have not been impacted by degradation.
PS low density	62.8 \pm 3.6	18.7 \pm 2.0	647.8 \pm 41.0	Biomass stock assumed to be similar to that of a PS of high degradation or 83% the stock in PS high density according to Hergoualc'h et al. (2017). Peat C stocks conservatively assumed to have not been impacted by degradation.
HS	0	0	628.3 \pm 67.3	Biomass and soil stocks from Draper et al. (2014) and Honorio Coronado et al. (2021), respectively.
HS formerly classified as PS	0	0	647.8 \pm 41.0	Biomass stock from Draper et al. (2014). Soil C stock assumed to be similar to that of a PS and to have not been impacted by deforestation.
PF	78.2 \pm 6.7	21.2 \pm 3.1	1,033.8 \pm 46.7	Values from Honorio Coronado et al. (2021)

272
 273
 274
 275
 276
 277
 278
 279
 280
 281
 282
 283
 284
 285
 286
 287
 288

289 **Table SI 7.** Peat CO₂-C emission factor (Mg C ha⁻¹ y⁻¹) per ecosystem and transition in the
 290 Peruvian Amazon. PS: Palm swamp, HS: Herbaceous swamp

291
 292 The peat flux rate per transition was the average of the emission factor before and after
 293 conversion. Whenever the class before conversion was an active C sink, the loss from removing
 294 the sink was also accounted for. For instance, over a transition from high density palm swamp
 295 (which absorbs at a rate of -1.8 M C ha⁻¹ y⁻¹) to medium density palm swamp (which absorbs at a
 296 rate of -0.3 M C ha⁻¹ y⁻¹), the soil absorbs at an average rate of -1.0 ± 1.4 Mg C ha⁻¹ y⁻¹ minus -1.8
 297 M C ha⁻¹ y⁻¹ which would have been absorbed in the absence of change.
 298

Ecosystem or transition	Peat emission factor[#]	Assumption and references
PS high density	-1.8 ± 1.8	Undegraded PS from Hergoualc'h et al. (accepted)
PS medium density	-0.3 ± 0.7	PS of medium degradation from Hergoualc'h et al. (accepted)
PS low density	6.0 ± 0.6	PS of high degradation from Hergoualc'h et al. (accepted)
HS formerly classified as PS	6.0 ± 0.6	Similar to PS low density
PS high density to PS medium density	0.7 ± 1.4	Average of uptake rate before and after conversion minus uptake occurring in the absence of transition
PS high density to PS low density / HS	3.9 ± 1.3	Average of uptake/emission rate before and after conversion minus uptake occurring in the absence of transition
PS medium density to PS low density / HS	3.2 ± 0.6	Average of uptake/emission rate before and after conversion minus uptake occurring in the absence of transition
PS low density to HS	6.0 ± 0.6	Average of emission rate before and after conversion

299 [#] A negative emission factor denotes an uptake of C, a positive emission factor an emission of C.

300 **Table SI 8. Error matrices**

301

302 Matrices for each year are presented first with pixel references, and then with pixel references adjusted for each class's area proportion
 303 within the landscape. The area-adjusted matrices were used to estimate accuracy. PS: Palm swamp, HS: Herbaceous swamp, PF: Pole
 304 forest, SFF: Seasonally Flooded Forest

305

306 Error matrix for year 2018

	PS high density	PS medium density	PS low density	HS	PF	SFF	Terra Firme Forest	Sand Bank	Pasture	Urban	Water	Secondary Forest
PS high density	747	72	6	0	12	3	1	0	0	0	0	0
PS medium density	150	688	150	0	15	2	3	0	0	0	0	0
PS low density	80	199	810	1	10	5	2	0	0	0	0	0
HS	0	0	0	963	0	1	0	0	7	4	0	0
PF	34	51	21	0	971	11	0	0	0	0	0	0
SFF	6	8	36	0	8	998	29	0	4	0	0	15
Terra Firme Forest	7	10	1	0	0	2	997	0	0	0	0	0
Sand Bank	0	0	0	0	0	0	0	491	0	11	0	0
Pasture	0	0	0	51	0	0	0	0	260	37	0	0
Urban	0	0	0	0	0	0	0	0	0	889	0	0
Water	0	0	0	0	0	0	0	103	0	0	1013	0
Secondary Forest	0	0	0	0	0	0	0	0	23	0	0	303

307

308 Error matrix, with values adjusted for area proportions for year 2018

	PS high density	PS medium density	PS low density	HS	PF	SFF	Terra Firme Forest	Sand Bank	Pasture	Urban	Water	Secondary Forest
PS high density	2.75E-02	2.65E-03	2.20E-04	0	4.40E-04	1.10E-04	3.68E-05	0	0	0	0	0
PS medium density	6.05E-03	2.78E-02	6.05E-03	0	6.10E-04	8.07E-05	1.21E-04	0	0	0	0	0
PS low density	4.31E-03	1.07E-02	4.36E-02	5.39E-05	5.40E-04	2.69E-04	1.08E-04	0	0	0	0	0

HS	0	0	0	1.66E-02	0.00E+00	1.72E-05	0	0	1.20E-04	6.89E-05	0	0
PF	6.60E-04	9.90E-04	4.10E-04	0	1.88E-02	2.13E-04	0	0	0	0	0	0
SFF	1.00E-03	1.33E-03	6.00E-03	0	1.33E-03	1.66E-01	4.83E-03	0	6.70E-04	0	0	2.50E-03
Terra Firme Forest	4.27E-03	6.10E-03	6.10E-04	0	0	1.22E-03	6.09E-01	0	0	0	0	0
Sand Bank	0	0	0	0	0	0	0	3.04E-03	0	6.81E-05	0	0
Pasture	0	0	0	5.48E-04	0	0	0	0	2.80E-03	3.98E-04	0	0
Urban	0	0	0	0	0	0	0	0	0	8.43E-04	0	0
Water	0	0	0	0	0	0	0	1.50E-03	0	0	1.48E-02	0
Secondary Forest	0	0	0	0	0	0	0	0	1.50E-04	0	0	1.95E-03

309
310

Error matrix for year 2007

	PS high density	PS medium density	PS low density	HS	PF	SFF	Terra Firme Forest	Sand Bank	Pasture	Urban	Water	Secondary Forest
PS high density	794	84	46	0	36	1	0	0	0	0	0	0
PS medium density	133	700	244	0	54	117	0	0	0	0	0	0
PS low density	79	159	616	13	11	52	1	0	0	0	19	0
HS	0	0	0	998	0	0	0	0	6	0	0	2
PF	14	60	31	0	710	13	0	0	0	0	0	0
SFF	4	9	65	0	198	771	7	0	1	0	0	249
Terra Firme Forest	3	2	7	0	0	55	998	0	0	0	0	0
Sand Bank	0	0	0	0	0	0	0	316	1	0	0	0
Pasture	0	0	0	0	0	0	0	0	65	0	0	4
Urban	0	0	0	0	0	0	0	0	3	1004	0	0

Water	0	0	0	0	0	0	0	0	0	0	0	985	0
Secondary Forest	0	0	0	0	0	0	0	0	0	0	0	0	120

311
312
313

Error matrix with adjusted for area proportions for year 2007

	PS high density	PS medium density	PS low density	HS	PF	SFF	Terra Firme Forest	Sand Bank	Pasture	Urban	Water	Secondary Forest
PS high density	3.17E-02	3.35E-03	1.84E-03	0	1.44E-03	3.99E-05	0	0	0	0	0	0
PS medium density	5.90E-03	3.11E-02	1.08E-02	0	2.40E-03	5.19E-03	0	0	0	0	0	0
PS low density	4.80E-03	9.65E-03	3.74E-02	7.89E-04	6.68E-04	3.16E-03	6.07E-05	0	0	0	1.15E-03	0
HS	0	0	0	1.53E-02	0	0	0	0	9.17E-05	0	0	3.06E-05
PF	2.14E-04	9.16E-04	4.73E-04	0	1.08E-02	1.98E-04	0	0	0	0	0	0
SFF	5.30E-04	1.19E-03	8.62E-03	0	2.63E-02	1.02E-01	9.28E-04	0	1.33E-04	0	0	3.30E-02
Terra Firme Forest	1.76E-03	1.18E-03	4.11E-03	0	0	3.23E-02	5.86E-01	0	0	0	0	0
Sand Bank	0	0	0	0	0	0	0	3.22E-03	1.02E-05	0	0	0
Pasture	0	0	0	0	0	0	0	0	2.66E-03	0	0	1.64E-04
Urban	0	0	0	0	0	0	0	0	1.77E-06	5.93E-04	0	0
Water	0	0	0	0	0	0	0	0	0	0	1.41E-02	0
Secondary Forest	0	0	0	0	0	0	0	0	0	0	0	1.11E-03

314
315
316

317 Error matrix, with adjusted for area proportions for year 1990

	PS high density	PS medium density	PS low density	HS	PF	SFF	Terra Firme Forest	Sand Bank	Pasture	Urban	Water	Secondary Forest
PS high density	329	41	21	2	22	8	2	0	14	0	10	0
PS medium density	379	878	112	0	6	1	2	0	1	0	6	0
PS low density	236	50	833	8	37	5	7	6	1	0	5	18
HS	0	2	4	803	1	0	0	0	8	0	12	0
PF	58	28	14	1	938	11	0	0	0	0	4	0
SFF	5	18	12	9	8	963	2	3	18	1	29	0
Terra Firme Forest	18	1	2	0	0	0	1017	2	0	0	0	31
Sand Bank	0	0	0	4	0	0	0	330	6	7	86	0
Pasture	0	0	0	57	0	5	2	0	202	42	0	0
Urban	0	0	0	44	0	0	0	29	44	912	61	1
Water	0	8	6	85	0	22	0	52	11	36	800	16
Secondary Forest	0	0	1	0	0	4	0	0	0	0	0	252

318

319

320 Error matrix, with adjusted for area proportions for year 1990

	PS high density	PS medium density	PS low density	HS	PF	SFF	Terra Firme Forest	Sand Bank	Pasture	Urban	Water	Secondary Forest
PS high density	2.36E-02	2.94E-03	1.51E-03	1.44E-04	1.58E-03	5.74E-04	1.44E-04	0	1.01E-03	0	7.18E-04	0
PS medium density	1.78E-02	4.11E-02	5.25E-03	0	2.81E-04	4.68E-05	9.37E-05	0	4.68E-05	0	2.81E-04	0
PS low density	1.42E-02	3.02E-03	5.02E-02	4.82E-04	2.23E-03	3.02E-04	4.22E-04	3.62E-04	6.03E-05	0	3.02E-04	1.09E-03
HS	0	4.16E-05	8.31E-05	1.67E-02	2.08E-05	0	0	0	1.66E-04	0	2.49E-04	0
PF	1.13E-03	5.47E-04	2.74E-04	1.95E-05	1.83E-02	2.15E-04	0	0	0	0	7.82E-05	0

SFF	5.76E-04	2.07E-03	1.38E-03	1.04E-03	9.21E-04	1.11E-01	2.30E-04	3.45E-04	2.07E-03	1.15E-04	3.34E-03	0
Terra Firme Forest	9.49E-03	5.27E-04	1.06E-03	0	0	0	5.36E-01	1.05E-03	0	0	0	1.63E-02
Sand Bank	0	0	0	6.89E-05	0	0	0	5.68E-03	1.03E-04	1.21E-04	1.48E-03	0
Pasture	0	0	0	8.53E-03	0	7.48E-04	2.99E-04	0	3.02E-02	6.29E-03	0	0
Urban	0	0	0	2.79E-04	0	0	0	1.84E-04	2.79E-04	5.79E-03	3.87E-04	6.34E-06
Water	0	2.85E-04	2.13E-04	3.02E-03	0	7.83E-04	0	1.85E-03	3.91E-04	1.28E-03	2.85E-02	5.69E-04
Secondary Forest	0	0	2.84E-05	0	0	1.14E-04	0	0	0	0	0	7.17E-03

321
322

323 **Table SI 9:** Area of peat-forming ecosystem (PS: Palm Swamp, HS: Herbaceous Swamp, PF: Pole forest) and their contribution to the
 324 total area of peat-forming ecosystems for studies conducted in the Peruvian Amazon. Areas of peat-forming ecosystems on peat are
 325 presented in bold italic in brackets for studies which identified peat occurrence by using a peat map (D, here)
 326

Ref.#	Area (Mha)					Contribution to study area of peat-forming ecosystems (%)			Share over peat (%)			Assumptions and methods regarding peatland area according to occurrence of peat-forming ecosystems
	Study	All peat-forming ecosystems <i>[on peat]</i>	PS	HS	PF	PS	HS	PF	PS	HS	PF	
A	13	3.6	2.8	0.4	0.4	78	12	10	100	100	100	Peat identified by the presence of peat-forming ecosystems. Peatland area computed as the area of peat-forming ecosystems
B	14	3.7	1.6	0.5	1.7	43	12	45	100	100	100	Same as for A
C	37.5	5.6	4.3	0.5	0.8	78	9	14				No peatland area assessed
D	78	6.1 <i>[6.2]</i>	4.7 <i>[4.6]</i>	0.7 <i>[0.7]</i>	0.7 <i>[0.7]</i>	77	11	12	99	98	99	Peat identified by a peat map from the study. Peatland area computed as the area of any vegetation category occurring on peat, including a small area of seasonally flooded forest (0.2Mha)
Here	28	6.9 <i>[5.1]</i>	5.5 <i>[4.2]</i>	0.6 <i>[0.4]</i>	0.8 <i>[0.5]</i>	79	9	11	76	59	63	Peat identified by a peat map (D). Peatland area computed as the area of peat-forming ecosystems over peat

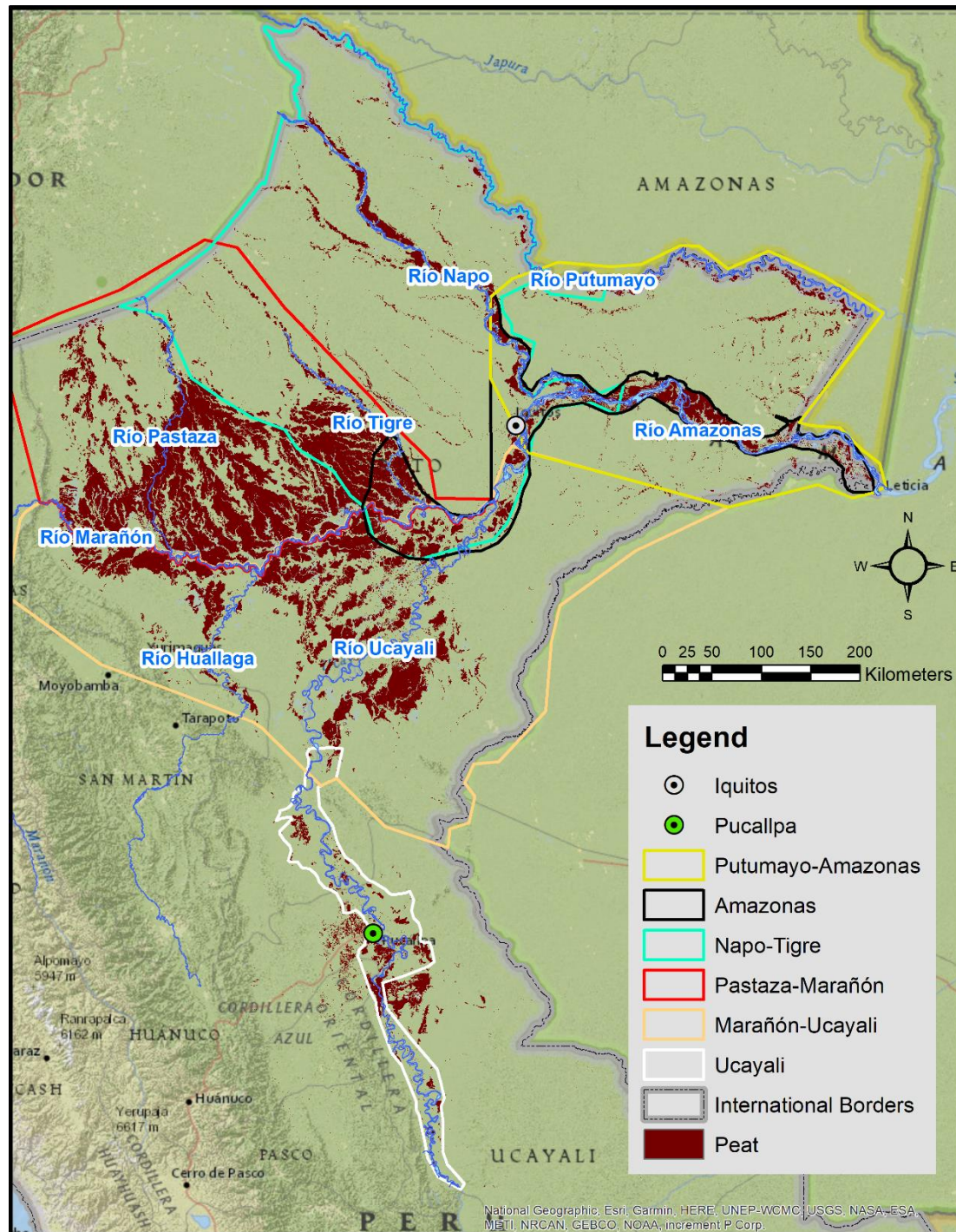
327 # References are A: Draper et al. (2014) in the Pastaza-Marañon Foreland Basin (PMFB), B: Bourgeau-Chavez et al. (2021) in the PMFB, C: Honorio Coronado
 328 et al. (2021) in the PMFB + along the Amazon and Napo rivers, D: Hastie et al. (2022) in the entire Peruvian Amazon

329 **Table SI 10:** Carbon stocks in the above-ground biomass and the soil of peat-forming ecosystem
 330 (PS: Palm Swamp, HS: Herbaceous Swamp, PF: Pole forest) over peat and their contribution to
 331 total peatland C stock.

332

Reference	C stock (Pg)			Contribution to total C stock			
	Total	PS	HS	PF	PS	HS	PF
Hastie et al. (2022)	5.7 [§]	4.2	0.7	0.8	74%	13%	14%
Here [#]	3.8	3.0	0.2	0.5	79%	6%	15%

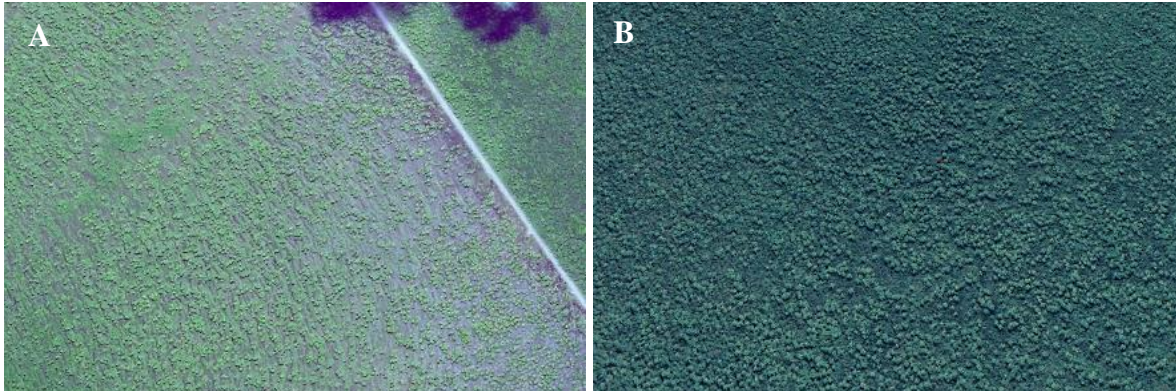
333 [§] The total peatland C stock of 5.8 Pg C estimated by Hastie et al. (2022) includes 0.1 Pg C in seasonally flooded
 334 forest on peat. [#] Excludes C stocks in the below-ground biomass presented in Table 6 for comparison with Hastie et
 335 al. (2022) who did not consider this pool.



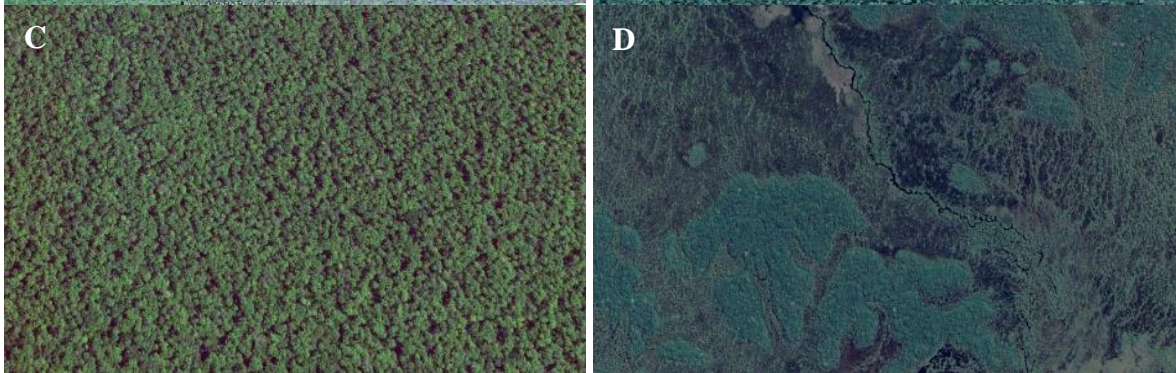
338
339

340 **Figure SI 1.** Study area showing peatlands (brown) according to Hastie et al. (2022). Six
341 stratified zones were used for classification: Putumayo-Amazonas, Amazonas, Napo-Tigre,
342 Pastaza-Marañón, Marañón-Ucayali, and Ucayali.

343



344

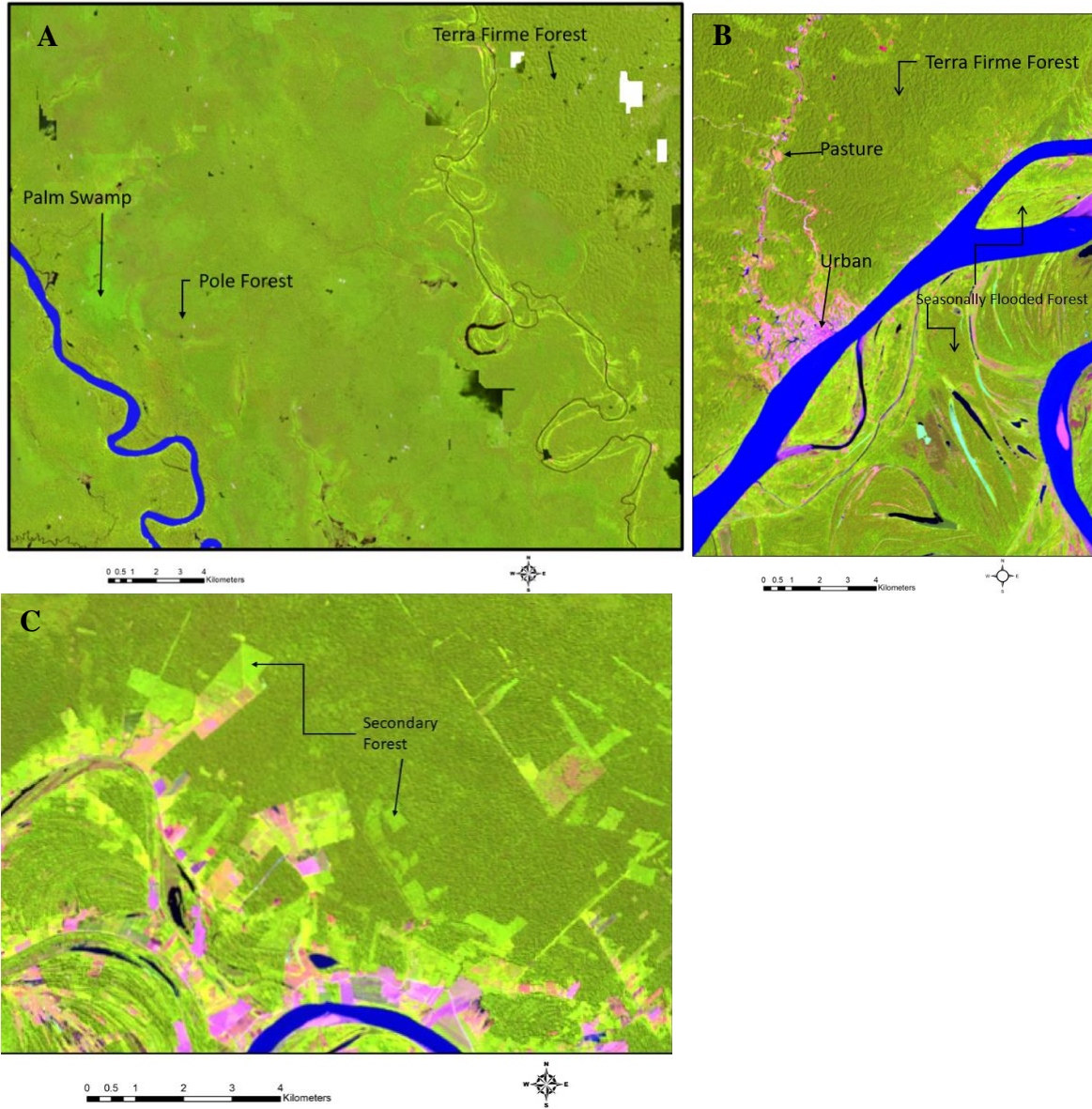


345



346

347 **Figure SI 2.** Google Earth (Google, 2021) images of different peat-forming land covers. A: low
348 density palm swamp, B: medium density palm swamp, C: high density palm swamp, D:
349 herbaceous swamp, E: Pole forest.

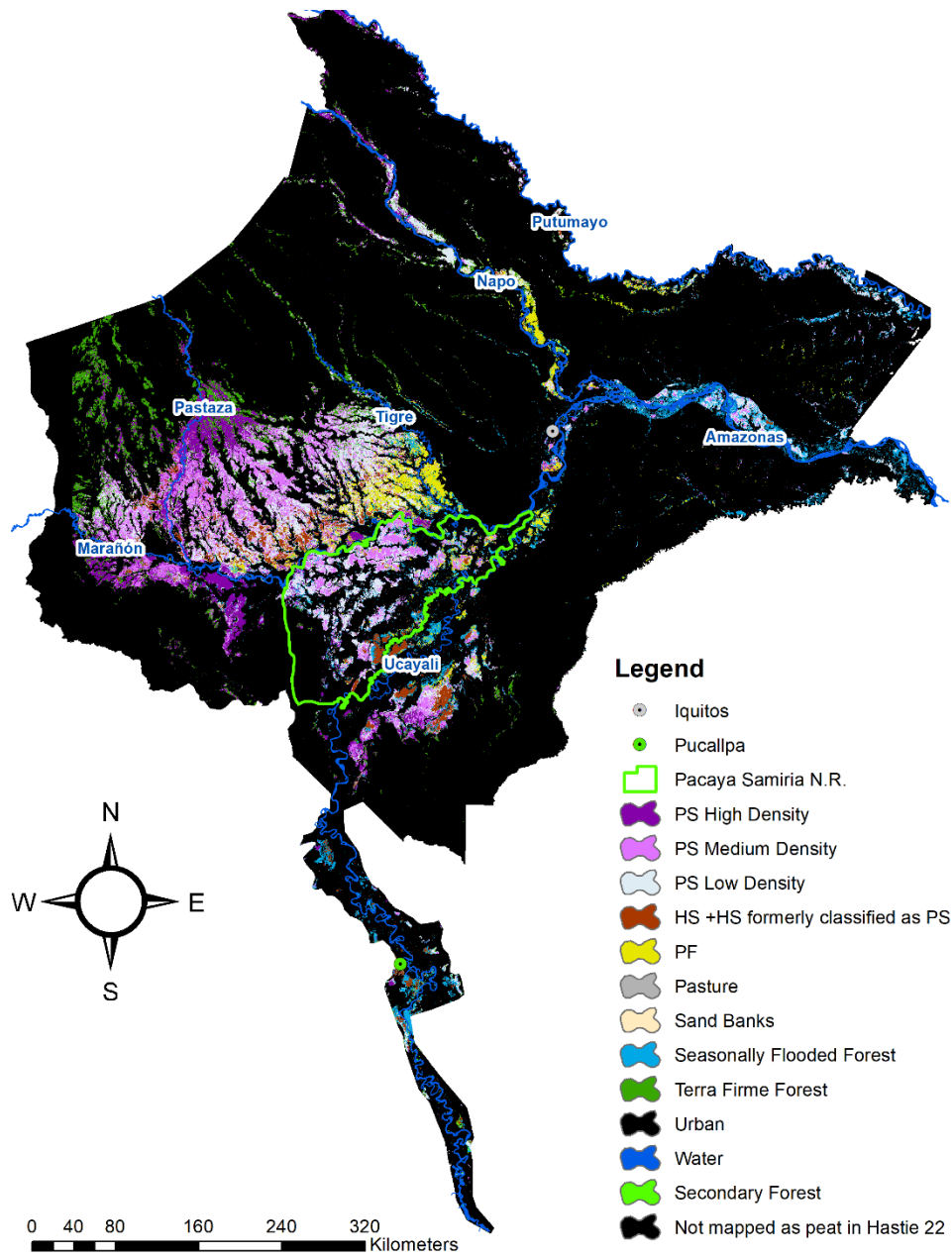


350

351

352

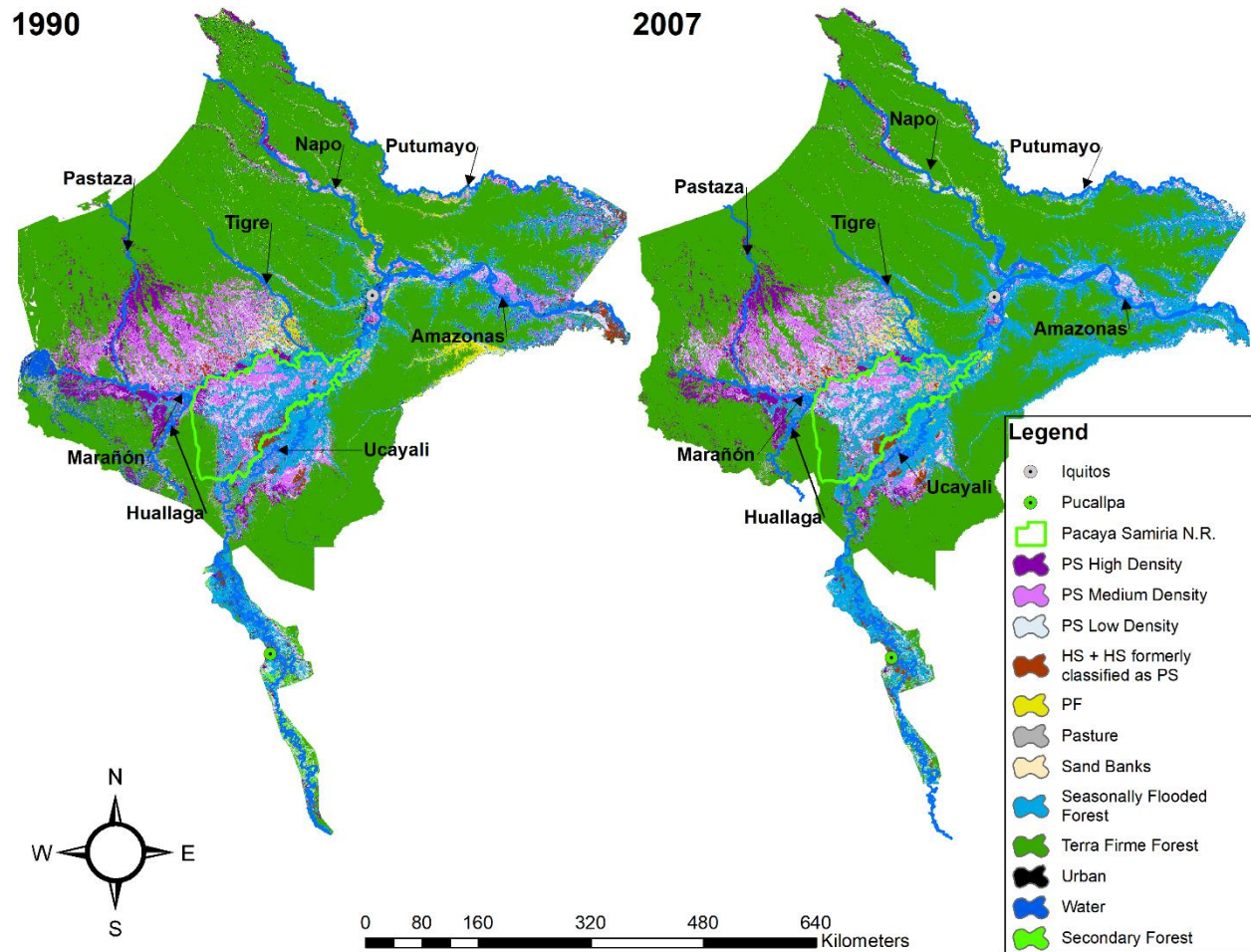
Figure SI 3. Land cover examples from Landsat Scene (Red Green Blue: 5, 4, 3)



353
 354
 355
 356
 357
 358
 359

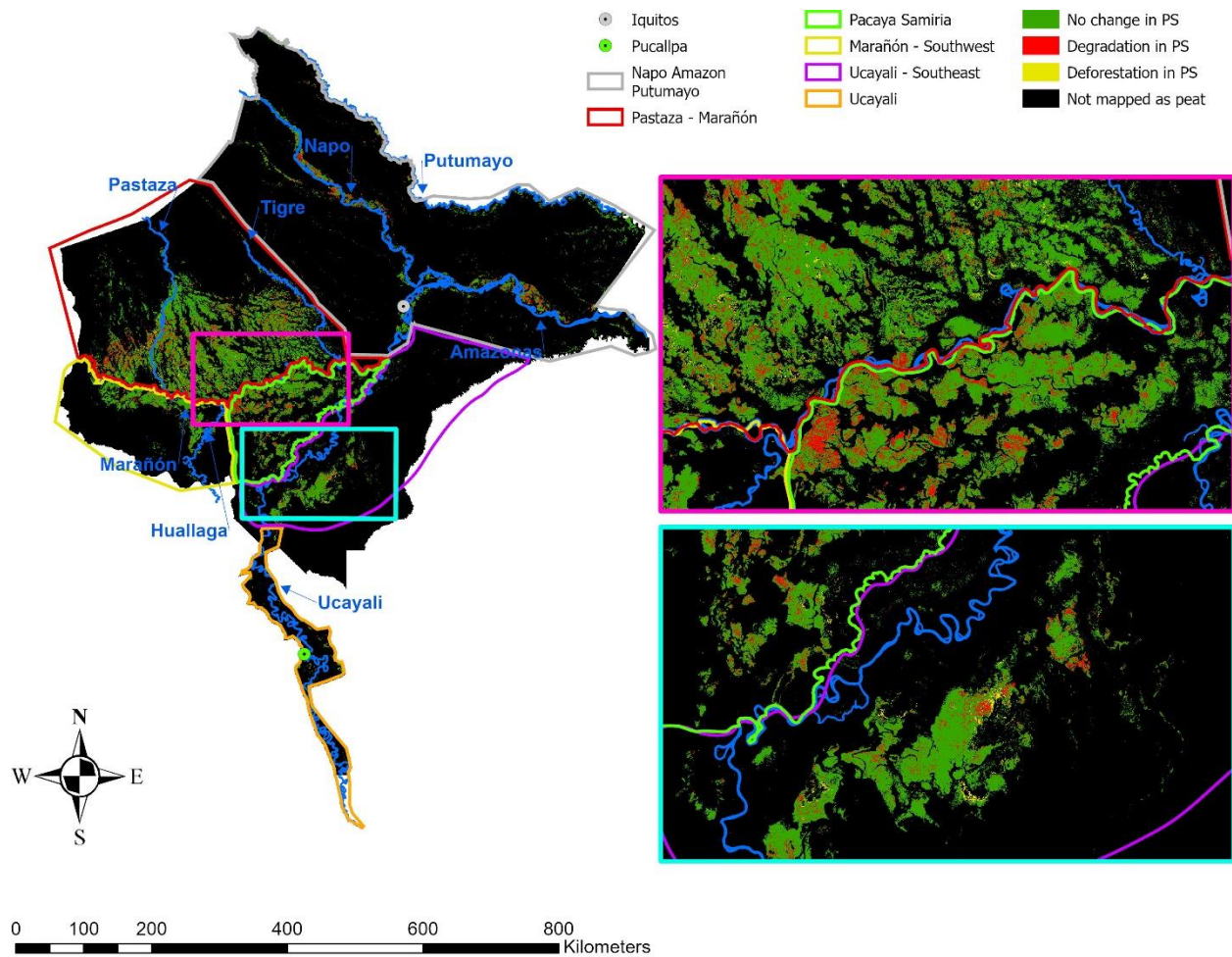
Figure SI 4. 2018 land cover map over peat

This map shows all of the land covers that overlapped peat, including non-peat-forming classes. Black areas were not mapped as peatlands by Hastie et al. (2022). PS: Palm swamp, HS: Herbaceous swamp, PF: Pole forest



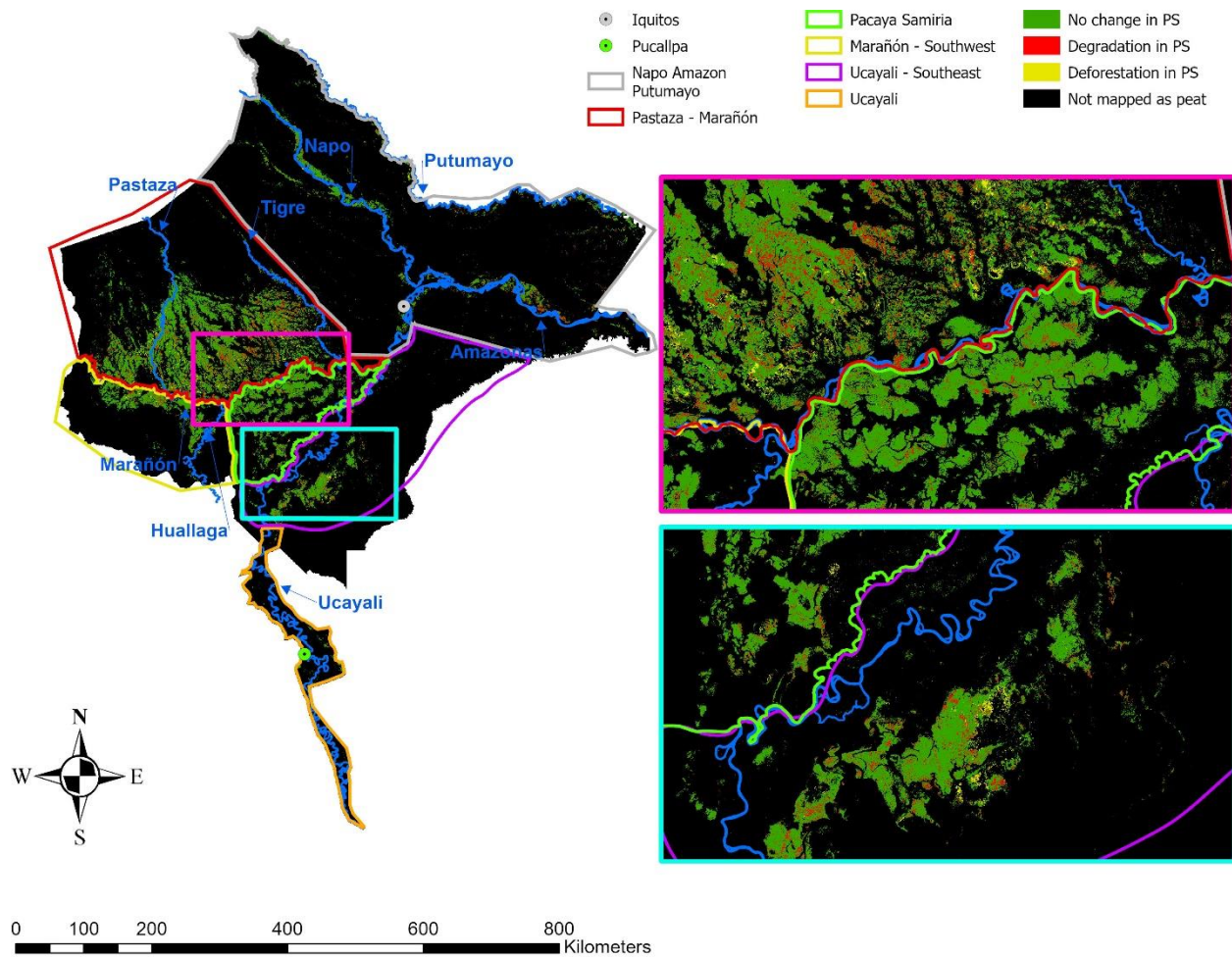
360
361
362

Figure SI 5. Land covers mapped for 1990 and 2007. PS: Palm swamp, HS: Herbaceous swamp, PF: Pole forest. HS classified as PS in former years was included in the HS class.



363
 364
 365
 366

Figure SI 6. Degradation and deforestation over peat observed in the 1990-2007 period. PS: Palm swamp, HS: Herbaceous swamp, PF: Pole forest



367
368

369 **Figure SI 7.** Degradation and deforestation over peat observed in the 2007-2018 period. PS:
 370 Palm swamp, HS: Herbaceous swamp, PF: Pole forest

References

Barbaran-Garcia, J. (2000). Cuantificación de biomasa y carbono en los principales sistemas de uso de suelo en Campo Verde. *Universidad Nacional de Ucayali*. Pucallpa, Peru.

Draper, F.C., Roucoux, K.H., Lawson, I.T., Mitchard, E.T.A., Honorio Coronado, E.N., Lahteenoja, O., Torres Montenegro, L., Valerrama Sandoval, E., Zarate, R., and Baker, T.R. (2014). The distribution and amount of carbon in the largest peatland complex in Amazonia. *Environmental Research Letters*. doi:10.1088/1748-9326/9/12/124017

Draper, F. C., Honorio Coronado, E. N., Roucoux, K. H., Lawson, I. T., Pitman, N. C. A., Fine, P. V. A., Phillips, O. L., Torres Montenegro, L. A., Valderrama Sandoval, E., Mesones, I., Garcia-Villacorta, R., Ramirez Arevelo, F. R., Baker, T. R. (2018). Peatland forests are the least diverse tree communities documented in Amazonia, but contribute to high regional beta diversity. *Ecography*. 41: 1256-1269. doi: 10.1111/ecog.03126

Endress, B.A., Horn, C. M., Gilmore, M. P. (2013). *Mauritia flexuosa* palm swamps: composition, Structure and implications for conservation and management. *Forest Ecol. Manag.* 302, 346–353. <http://dx.doi.org/10.1016/j.foreco.2013.03.051>

Fujisaka, S., Escobar, G., Veneklaas, E.J. (2000). Weedy fields and forests: interactions between land use and the composition of plant communities in the Peruvian Amazon. *Agric. Ecosyst. Environ.* 78. 175-186. [https://doi.org/10.1016/S0167-8809\(99\)00122-X](https://doi.org/10.1016/S0167-8809(99)00122-X)

Garcia-Villacorta, R., Ahuite-Reátegui, M., & Olortegui-Zumaeta, M. (2003). Clasificación de bosques sobre arena blanca de la Zona Reservada Allpahuayo-Mishana. *Folia Amazónica*, 14(1), 17-33.

Google. (2021). Google earth. Retrieved from <https://earth.google.com/>.

Gutiérrez-Velez, V.H., DeFries, R. (2013). Annual multi-resolution detection of land cover conversion to oil palm in the Peruvian Amazon. *Remote Sensing of Environment*. 129: 154-167.

Gutierrez-Velez V.H., Rodriguez, J., Lara, W., Sarmiento, V. (2021). Probabilistic approximation to change and no change in multispectral remote sensing. *International Journal of Remote Sensing*. 42:19, 7428-7453. <https://doi.org/10.1080/01431161.2021.1958391>

Hastie, A., Honorio Coronado, E. N., Reyna, J., Mitchard, E. T. A., Akesson, C. M., Baker, T. R., Cole, L. E. S., Cordova Oroche, C. J., Dargie, G., Davila, N., De Grandi, E. C., Del Aguila, J., del Castillo Torres, D., De La Cruz Paiva, R., Draper, F. C., Flores, G., Grandez, J., Hergoualc'h, K., Householder, J. E., Janovec, J. P., Lahteenoja, O., Reyna, D., Rodriguez-Veiga, Pedro, Roucoux, K. H., Tobler, M., Wheeler, C. E., Williams, M., Lawson, I. T., (2022). Risks to carbon storage from land-use change revealed by peat thickness maps of Peru. *Nature Geoscience*. <https://doi.org/10.1038/s41561-022-00923-4>

Hergoualc'h, K., Gutierrez-Velez, V. H., Menton, M., and Verchot, L. V. (2017). Characterizing degradation of palm swamp peatlands from space and on the ground: An exploratory study in the Peruvian Amazon. *Forest Ecology and Management*. 393. 63-73.
<http://dx.doi.org/10.1016/j.foreco.2017.03.016>

Hijmans, R.J. (2020). Raster: Geographic Data Analysis and Modeling. R package version 3.3 13. <https://CRAN.R-project.org/package=raster>

Holm, J.A., Miller, C. J., Cropper, W. P. (2008). Population dynamics of the dioecious Amazon palm *Mauritia flexuosa*: simulation analysis of sustainable harvesting. *Biotropica* 40, 550–558.
10.1111/J.1744-7429.2008.00412

Honorio Coronado, E. N., Hergoualc'h, K. (2021). Informe sobre los análisis y resultados de las emisiones de CO2 debido a la deforestación y degradación de turberas en la Amazonía peruana. *CIFOR report*
<https://data.cifor.org/dataset.xhtml?persistentId=doi:10.17528/CIFOR/DATA.00269>

Horn, C. M., Gilmore, M. P., Endress, B. A. (2012). Ecological and socio-economic factors influencing aguaje (*Mauritia flexuosa*) resource management in two indigenous communities in the Peruvian Amazon. *Forest Ecology and Management*. 267. 93-103.
doi:10.1016/j.foreco.2011.11.040

JAXA. Japanese Aerospace Exploration Agency. Accessed from:
<https://www.eorc.jaxa.jp/ALOS/en/index.htm>

Leutner, B., Horning, N., and Schwalb-Willmann, J. (2019). RStoolbox: Tools for Remote Sensing Data Analysis. R package version 0.2.6. <https://CRAN.Rproject.org/package=RStoolbox>

Marengo, J.A. (1998). Climatología de la zona de Iquitos, Perú. 114. *Annales Universitatis Turkuensis Ser A II*, pp. 35–57.

Matricardi, E.A.T., Skole, D.L., Pedlowski, M.A., Chomentowski, W., Fernandes, L.C. (2010). Assessment of tropical forest degradation by selective logging and fire using Landsat imagery. *Remote Sensing of Environment*. 114. 1117-1129. doi:10.1016/j.rse.2010.01.001

NASA JPL (2013). NASA Shuttle Radar Topography Mission Global 1 arc second [Data set]. NASA EOSDIS Land Processes DAAC. Accessed from:
<https://doi.org/10.5067/MEaSURES/SRTM/SRTMGL3.003>

Olofsson, P., Foody, G.M., Herold, M., Stehman, S.V., Woodcock, C.E., Wulder, M.A. (2014). Good practices for estimating area and assessing accuracy of land change. *Remote Sensing of Environment*. 148. 42-57. <http://dx.doi.org/10.1016/j.rse.2014.02.015>

Palacios, J., Zarate, R., Torres, G., Denux, J-P., Maco, J., Gallardo, G., Mori, T., Rengifo, J., Jarama, A., Marin, M., Garcia, F., Cuadros, A. (2016). Mapeo de los bosques tipo varillal utilizando imágenes de satélite Rapideye en la provincia Maynas, Loreto, Peru. *Instituto de Investigaciones de la Amazon Peruana*. Vol. 25. 25-36.

Potapov, P., Li, X., Hernandez-Serna, A., Tyukavina, A., Hansen, M.C., Kommareddy, A., Pickens, A., Turubanova, S., Tang, H., Silva, C.E., Armston, J., Dubayah, R., Blair, J. B. Hofton, M. (2020). Mapping and monitoring global forest canopy height through integration of GED and Landsat data. *Remote Sensing of Environment*, 112165.

Roberts, D. A., Numata, I., Holmes, K., Batista, G., Krug, T., Monteiro, A., et al. (2002). Large area mapping of land-cover change in Rondonia using multitemporal spectral mixture analysis and decision tree classifiers. *Journal of Geophysical Research*, 107, 1–8.

<https://doi.org/10.1029/2001JD000374>